Liquid Crystals
Publication details, including instructions for authors and subscription information:
http://www.informaworld.com/smpp/title~content=t713926090

Use of a hybrid pseudospectral time-domain-finite-difference time-domain method for optical simulation of liquid crystals

Yun Fang[a]; Xi Li[b]; Jian Zhang[a]; Liying Wu[a]
[a] Institute of Ultra-Precision Optoelectronic Instrument Engineering, Harbin Institute of Technology, Harbin, China [b] Department of Precision Machinery and Instrumentation, University of Science and Technology of China, Hefei, China

Online publication date: 04 March 2010

To cite this Article Fang, Yun , Li, Xi , Zhang, Jian and Wu, Liying(2010) 'Use of a hybrid pseudospectral time-domain-finite-difference time-domain method for optical simulation of liquid crystals', Liquid Crystals, 37: 3, 241 — 246
To link to this Article: DOI: 10.1080/02678290903242950
URL: http://dx.doi.org/10.1080/02678290903242950

Liquid Crystals,
Vol. 37, No. 3, March 2010, 241–246

Taylor & Francis
Taylor & Francis Group

Use of a hybrid pseudospectral time-domain–finite-difference time-domain method for optical simulation of liquid crystals

Yun Fang[a]*, Xi Li[b], Jian Zhang[a] and Liying Wu[a]

[a]*Institute of Ultra-Precision Optoelectronic Instrument Engineering, Harbin Institute of Technology, Harbin, 150001, China;* [b]*Department of Precision Machinery and Instrumentation, University of Science and Technology of China, Hefei, 230026, China*

(Received 13 November 2008; final version received 7 August 2009)

In order to reduce the computational cost of the finite-difference time-domain method, the pseudospectral time-domain method is applied to the glass substrate direction with a large surface and smooth internal media, while the finite-difference time-domain method is applied to the thickness direction of a cell with a small thickness and fine structures. A fast Fourier transform algorithm, instead of the central-difference in the finite-difference time-domain method, is used to represent the spatial derivatives in the pseudospectral time-domain method, which greatly reduces the spatial sampling rate in the glass substrate direction. Both the hybrid method and the finite-difference time-domain method are used to simulate the propagation of light through the same twisted nematic pixel in the on state for 100 fs. The maximum deviation of the transmittance obtained using both methods is less than 5.1%; the memory capacity and computational time required for the hybrid method are about 8.5% and 21% respectively compared with those required for the finite-difference time-domain method. The use of the hybrid method reduces the memory capacity and computational time required for the finite-difference time-domain method while its accuracy is preserved.

Keywords: liquid crystal; optical simulation; finite-difference time-domain method; pseudospectral time-domain method

1. Introduction

Liquid crystals are widely used in displays and photonics devices. Optical simulation is an effective tool by which the optical properties of these devices can be analysed. Traditional matrix-type solvers, based on the stratified-medium approximation, are the most widely used methods, but they can be applied to one-dimensional structures only [1–3]. Other methods, such as the geometrical optics approximation method [4], the grating method [5] and the beam propagation method [6], are capable of dealing with multi-dimensional structures, but they introduce approximations at the mathematical level, and lead to not only high numerical efficiency but also such limitations as small incident angle or low accuracy.

The finite-difference time-domain (FDTD) method was introduced by Yee in 1966 [7]. It is a simple, robust and powerful numerical technique which can be used for the rigorous solution of Maxwell equations. It has also been used to simulate the propagation of light through liquid crystals [8, 9]. In the Yee-type FDTD method, the electric field components and magnetic field components are located in different positions in a staggered manner, and they are also interleaved in a leapfrog time-stepping scheme. Second-order accuracy central-differences are used to represent the derivatives with respect to both space and time. However, the accuracy of the FDTD method is limited by the spatial sampling rate due to the numerical dispersion effect. For a prescribed accuracy, the spatial sampling rate is determined by the minimum wavelength λ_{min} of an incident wave, the size l of the significant structural details and the electrical size of the structure being modelled. Numerous examples indicate that the acceptable results of the FDTD method for an electrically small problem require a spatial sampling rate of at least 10 to 20 cells per $\min\{\lambda_{min}, l\}$. This sampling rate should be further increased for an electrically large problem. This makes the modelling of electrically large problems by the FDTD method very difficult because of the memory requirements [10].

One of the ways to reduce the numerical dispersion of the Yee-type FDTD method is the Fourier pseudospectral time-domain (PSTD) method proposed by Liu [11]. Unlike the FDTD method, the electric field components and magnetic field components in the PSTD method are located in the same position in an unstaggered manner. This unstaggered grid arrangement has an important advantage over the staggered grid arrangement of the FDTD method for anisotropic media [12]. A fast Fourier transform (FFT) algorithm is used to represent the spatial derivatives

*Corresponding author. Email: hit_fangyun@yahoo.com.cn

ISSN 0267-8292 print/ISSN 1366-5855 online

DOI: 10.1080/02678290903242950
http://www.informaworld.com

in the PSTD method. Accurate results can be obtained for a problem with smooth internal media using the PSTD method only at a spatial sampling rate of 2 cells per $\min\{\lambda_{\min}, l\}$. The spatial sampling rate of the PSTD method is determined by $\lambda_{\min}$ and l, regardless of the overall electrical size of the structure being modelled. For an electrically large problem which does not have any structural detail finer than $\lambda_{\min}/2$, the PSTD method can be used to achieve a reduction of $4^D - 8^D$ in computational cost compared with the FDTD method, where D is the number of dimensions. However, the advantage of the PSTD method is not so evident for problems with any structural detail finer than $\lambda_{\min}/8$ and/or with small electrical size. In addition, it is difficult to treat high-contrast materials by using the Fourier PSTD method. Non-physical results can be obtained using the PSTD method for a problem with abrupt jumps in permittivity and/or permeability.

In short, the FDTD method is suitable for the modelling of an electrically small problem with fine structural details, while the PSTD method is suitable for the modelling of an electrically large problem with smooth internal media. Liquid crystal cells are a kind of thin plate with a small thickness and fine structures in the thickness direction of a cell, and a large surface and smooth internal media in the glass substrate direction. Several researchers have suggested that the FDTD and PSTD methods be combined for structures of this kind of thin plate, so that different methods can be applied to different directions to reduce the memory capacity and computation time required for the FDTD method while its accuracy is preserved [13–15]. In addition, it is easier to introduce a plane wave by applying the total-field/scattered-field (TF/SF) technique to the thickness direction of a cell in the FDTD method. For simplicity, we restrict our derivation to a two-dimensional (2D) structure and limit the material used to non-magnetic material.

2. Implementation of a hybrid PSTD–FDTD method

The general form of the Maxwell equations for the propagation of light within liquid crystals can be expressed as

$$\frac{\partial \boldsymbol{D}}{\partial t} = \nabla \times \boldsymbol{H}, \tag{1a}$$

$$\frac{\partial \boldsymbol{H}}{\partial t} = -\frac{1}{\mu_0}\nabla \times \boldsymbol{D}, \tag{1b}$$

$$\boldsymbol{D} = \epsilon_0 \boldsymbol{\epsilon}_{\mathrm{r}} \cdot \boldsymbol{E}, \tag{1c}$$

where μ_0 is the free-space magnetic permeability, ϵ_0 is the free-space permittivity and $\boldsymbol{\epsilon}_r$ is the relative dielectric tensor determined by the liquid crystal director (n_x, n_y, n_z).

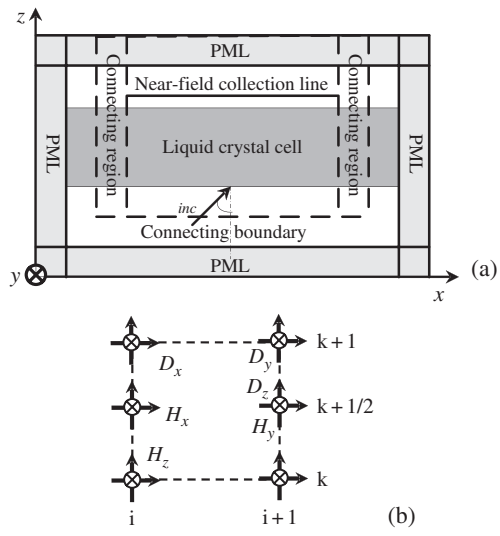

Figure 1. Schematic views of (a) the computational space and (b) the computational cell for the 2D hybrid PSTD–FDTD method.

As shown in Figure 1(a), the split-field material-independent perfectly matched layers (PMLs) based on the ($\boldsymbol{D}$, $\boldsymbol{H}$) fields, as reported in [16], are applied to terminate the computational area. The generalised TF/SF technique, which combines the TF/SF technique [10] of the FDTD method and the weighted TF/SF technique [17] of the PSTD method, is used to introduce a plane wave into the computational grid. The dashed line/rectangle represents the connecting boundary/region between the total-field and scattered-field regions. The electric flux density $\boldsymbol{D}$ and the magnetic fields $\boldsymbol{H}$ are interleaved in a leapfrog time-stepping scheme, and the sampling interval is half a time step, $\Delta t/2$. As shown in Figure 1(b), $\boldsymbol{D}$ and $\boldsymbol{H}$ are staggered in the z direction, but unstaggered in the x direction. Δx and Δz are the grid size in the x and z directions, respectively. In addition, the electric fields $\boldsymbol{E}$ are located at the same position as $\boldsymbol{D}$.

2.1 Discretisation

In the 2D hybrid PSTD–FDTD method, the FDTD method is applied to the z direction while the PSTD method is applied to the x direction. Considering the invariance in the y direction ($\partial/\partial y = 0$), the time-domain update equations can be derived as

$$D_x|_{i,k}^{n+1} = D_x|_{i,k}^{n} - \frac{\Delta t}{\Delta z}\left(H_y|_{i,k+\frac{1}{2}}^{n+\frac{1}{2}} - H_y|_{i,k-\frac{1}{2}}^{n+\frac{1}{2}}\right), \tag{2a}$$

$$D_y|_{i,k}^{n+1} = D_y|_{i,k}^{n} + \Delta t \left(\frac{H_x|_{i,k+\frac{1}{2}}^{n+\frac{1}{2}} - H_x|_{i,k-\frac{1}{2}}^{n+\frac{1}{2}}}{\Delta z} - \Im_x^{-1}\left\{j2\pi f_x \Im_x\left[H_z^{n+\frac{1}{2}}(i,k)\right]\right\}\right), \tag{2b}$$

$$D_z|_{i,k+\frac{1}{2}}^{n+1} = D_z|_{i,k+\frac{1}{2}}^{n} + \Delta t \Im_x^{-1}\left\{ j2\pi f_x \Im_x \left[H_y^{n+\frac{1}{2}}\left(i, k+\frac{1}{2}\right)\right]\right\} \quad (2c)$$

and

$$H_x|_{i,k+\frac{1}{2}}^{n+\frac{1}{2}} = H_x|_{i,k+\frac{1}{2}}^{n-\frac{1}{2}} + \frac{\Delta t}{\mu_0 \Delta z}\left(E_y|_{i,k+1}^{n} - E_y|_{i,k}^{n}\right), \quad (3a)$$

$$H_y|_{i,k+\frac{1}{2}}^{n+\frac{1}{2}} = H_y|_{i,k+\frac{1}{2}}^{n-\frac{1}{2}} - \frac{\Delta t}{\mu_0}\left(\frac{E_x|_{i,k+1}^{n} - E_x|_{i,k}^{n}}{\Delta z} - \Im_x^{-1}\left\{ j2\pi f_x \Im_x \left[E_z^{n}\left(i, k+\frac{1}{2}\right)\right]\right\}\right), \quad (3b)$$

$$H_z|_{i,k}^{n+\frac{1}{2}} = H_z|_{i,k}^{n-\frac{1}{2}} - \frac{\Delta t}{\mu_0}\Im_x^{-1}\left\{ j2\pi f_x \Im_x \left[E_y^{n}(i,k)\right]\right\}, \quad (3c)$$

where n is the number of time steps, and i and k are the indices of the grid points in the x and z directions, respectively. $\Im$ denotes the FFT operator, $f_x = m/(N\Delta x)$ $(m = -N/2, ..., N/2)$ and $N = IE$ is the grid number in the x direction.

The relationship between the components $\boldsymbol{E}$ and $\boldsymbol{D}$ is as follows:

$$E_x|_{i,k}^{n+1} = \epsilon_0^{-1}\left(\epsilon_{xx}^{-1}|_{i,k} D_x|_{i,k}^{n+1} + \epsilon_{xy}^{-1}|_{i,k} D_y|_{i,k}^{n+1} + \epsilon_{xz}^{-1}|_{i,k} D_z|_{i,k}^{n+1}\right), \quad (4a)$$

$$E_y|_{i,k}^{n+1} = \epsilon_0^{-1}\left(\epsilon_{yx}^{-1}|_{i,k} D_x|_{i,k}^{n+1} + \epsilon_{yy}^{-1}|_{i,k} D_y|_{i,k}^{n+1} + \epsilon_{yz}^{-1}|_{i,k} D_z|_{i,k}^{n+1}\right), \quad (4b)$$

$$E_z|_{i,k+\frac{1}{2}}^{n+1} = \epsilon_0^{-1}\left(\epsilon_{zx}^{-1}|_{i,k+\frac{1}{2}} D_x|_{i,k+\frac{1}{2}}^{n+1} + \epsilon_{zy}^{-1}|_{i,k+\frac{1}{2}} D_y|_{i,k+\frac{1}{2}}^{n+1} + \epsilon_{zz}^{-1}|_{i,k+\frac{1}{2}} D_z|_{i,k+\frac{1}{2}}^{n+1}\right), \quad (4c)$$

where $\epsilon_{pq}^{-1}(p, q = x, y, z)$ is the inverse matrix components of $\boldsymbol{\epsilon}_r$.

To avoid numerical instability, the time step has a specific bound related to the grid size. The numerical stability and dispersion characteristics of the hybrid PSTD–FDTD method can be built through eigenvalue analysis for arbitrary anisotropic media [18, 19]; however, it is difficult to have an analytic solution for this type of media. The stability of an isotropic case always provides upper bounds for the stability of the arbitrary anisotropic case [18, 20]. Therefore, the upper bounds for the stability of anisotropic media satisfy the following equation [13]:

$$\Delta t \le \frac{2}{c_0\sqrt{(\pi/\Delta x)^2 + (2/\Delta z)^2}} \quad (5)$$

where c_0 is the speed of light in free space.

2.2 *Incident wave sources*

For the generalised TF/SF technique, the electromagnetic fields in the entire computational space can be expressed as

$$\boldsymbol{E} = \boldsymbol{E}_{\text{scat}} + \zeta \boldsymbol{E}_{\text{inc}} \quad (6a)$$

$$\boldsymbol{H} = \boldsymbol{H}_{\text{scat}} + \zeta \boldsymbol{H}_{\text{inc}} \quad (6b)$$

where ζ stands for the weight of the incident fields.

As shown in Figure 2(a), $i = i_{a2}$ and $i = i_{b2}$ are the connecting boundaries between the scattered-field and total-field regions in the FDTD method; $i = (i_{a1}, \ldots, i_{a2})$ and $i = (i_{b2}, \ldots, i_{b1})$ are the connecting regions between the scattered-field and total-field regions in the PSTD method. The smooth connecting regions in the PSTD method eliminate the Gibbs effect during the FFT calculation of the fields with abrupt jumps [17]. For the 2D hybrid PSTD–FDTD method, the generalised TF/SF technique combines the TF/SF and weighted TF/SF techniques for the plane-wave excitations. Unlike the scattering problems in microwaves, the problems in optics emphasise more the properties of transmittance, polarisation and diffraction. Therefore, the upper connecting boundary is extended into the upper boundary of the computational space. As shown in Figure 2(b), $(i = i_{a1}, \ldots, i_{b1}; k = k_a)$

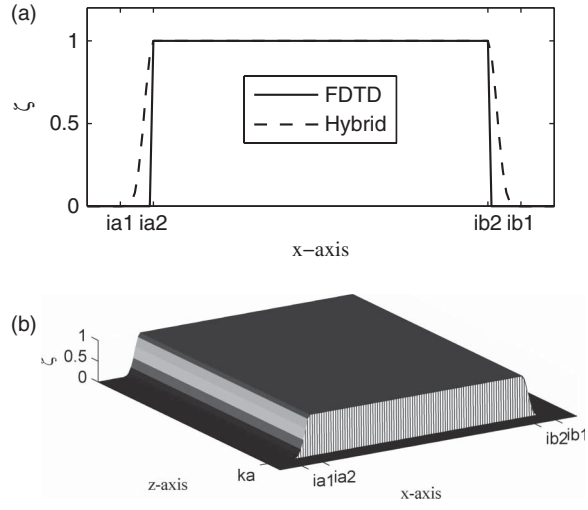

Figure 2. Distribution of the weighting function of the incident fields for (a) the 1D FDTD and PSTD methods and (b) the 2D hybrid PSTD–FDTD method. $\zeta = 0$ is the scattered-field region, $\zeta = 1$ is the total-field region, and $0 < \zeta < 1$ is the connecting region.

is the connecting boundary, $(i = i_{a1}, \ldots, i_{a2}; k = k_a, \ldots, KE)$ and $(i = i_{b2}, \ldots, i_{b1}; k = k_a, \ldots, KE)$ are the connecting regions and KE is the grid number in the z direction.

To maintain the consistency of the numerical differentiation on the connecting boundary/region, a correction term related to the incident fields on the boundary/region is applied. The correction of D_y on the lower connecting boundary $(i = i_{a1}, \ldots, i_{b1}; k = k_a)$ and the left connecting region $(i = i_{a1}, \ldots, i_{a2}; k = k_a, \ldots, KE)$ is taken as an example to illustrate the correction of the FDTD and PSTD methods. On the lower connecting boundary $(i = i_{a1}, \ldots, i_{b1}; k = k_a)$, the correction equation for D_y satisfies the following equation:

$$D_y|_{i,k_a}^{n+1} = \{D_y|_{i,k_a}^{n+1}\} - \frac{\Delta t}{\Delta z}\zeta|_i H_{x,inc}|_{i,k_a-\frac{1}{2}}^{n+\frac{1}{2}}. \quad (7)$$

On the left connecting region $(i = i_{a1}, \ldots, i_{a2}; k = k_a, \ldots, KE)$, the correction equation for D_y satisfies the following:

$$D_y|_{i,k}^{n+1} = \{D_y|_{i,k}^{n+1}\} + \Delta t \frac{\partial \zeta}{\partial x}|_i H_{z,inc}|_{i,k}^{n+\frac{1}{2}}. \quad (8)$$

In Equations (7) and (8), the term $D_y|_{i,k}^{n+1}$ on the left-hand side denotes the field after correction, and the first term on the right-hand side denotes the field before correction, while the second term denotes the correction term related to the incident fields. The derivative $\partial\zeta/\partial x$ is calculated through the FFT.

On the lower connecting boundary, the incident fields required for the correction can be obtained by direct calculation or interpolation. However, it is difficult to obtain the precise values of the incident fields on either the left or right connecting regions for they contain inhomogeneous anisotropic media and the fields between neighbour grids interact with each other along the x direction. Nonetheless, we could assume that the orientation of the liquid crystal director varies little between neighbour grids along the x direction due to the viscosity of the liquid crystals. On this assumption, the calculation of the incident fields on either the left or right connecting regions is approximated by the calculation of the incident fields for layered anisotropic media, and this can be done by creating some split-field 1D auxiliary FDTD grids along the z direction [21].

3. Numerical validation

To validate the effectiveness of the hybrid PSTD–FDTD method, the optical properties of a twisted nematic (TN) pixel in the on state are analysed. The results are compared with those obtained using the FDTD and Berreman methods. As shown in Figure 3, a gradient-index anti-reflection coating is applied to minimise the effect of the air–glass interface. The parameters of the liquid crystals are $K_1 = 12.5 \times 10^{-12}$ N, $K_2 = 7.3 \times 10^{-12}$ N, $K_3 = 17.9 \times 10^{-12}$ N, $\epsilon_{\parallel} = 14.1$, $\epsilon_{\perp} = 4.09$, $n_o = 1.5$ and $n_e = 1.6$. The refractive index of glass is 1.5.

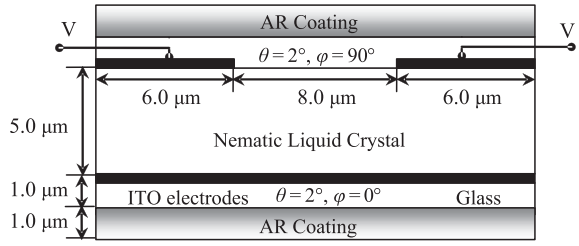

Figure 3. The twisted nematic pixel geometry with physical dimensions and liquid crystal material alignment.

The incident wave is a y-polarised monochromatic plane-wave with $\lambda = 632.8$ nm from the bottom of a liquid crystal cell. The thicknesses of the PMLs in the x and z directions are both 20 cells. For the FDTD method, the same grid size is assumed in the x and z directions, that is, $\Delta x = \Delta z = \Delta = \lambda/40$. The sampling interval of the time step is $\Delta t = \Delta/(3c_0)$. Whereas for the hybrid PSTD–FDTD method we choose an appropriate Δx which is less than $\lambda/2$ and makes the grid number in the x direction satisfy the requirement of 2^N (N is integral number), here $\Delta x = \lambda/2.88$. In addition, the hybrid PSTD–FDTD and FDTD methods have the same Δz and Δt .

The director orientation changes when a voltage is applied to the TN pixel. As shown in Figure 4, the director distribution obtained by applying a voltage of $V = 3$ V is inhomogeneous in both the x and z directions. Here, it is calculated using the LC3D software from Liquid Crystal Institute, Kent State University [22].

The director causes a change in intensity and phase of the incident fields as it passes through the director. As shown in Figure 5(a), the intensity of E_y reduces when

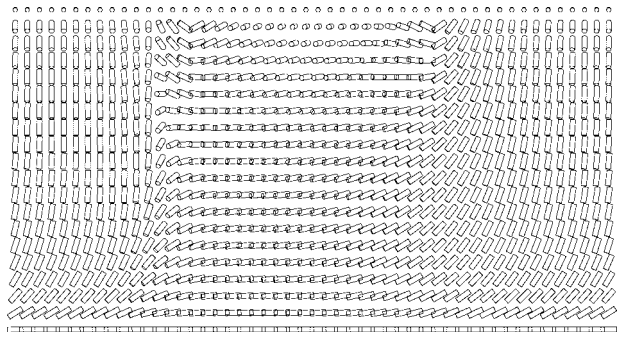

Figure 4. The director profile at $V = 3$ V.

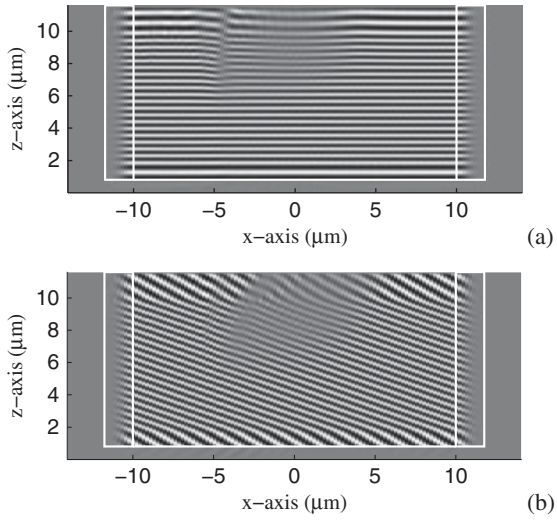

Figure 5. Snapshots of the electric field E_y for the TN pixel in the on state ($V = 3$ V) at (a) normal incidence and (b) 30° incidence. y-polarised incident light with $\lambda = 632.8$ nm.

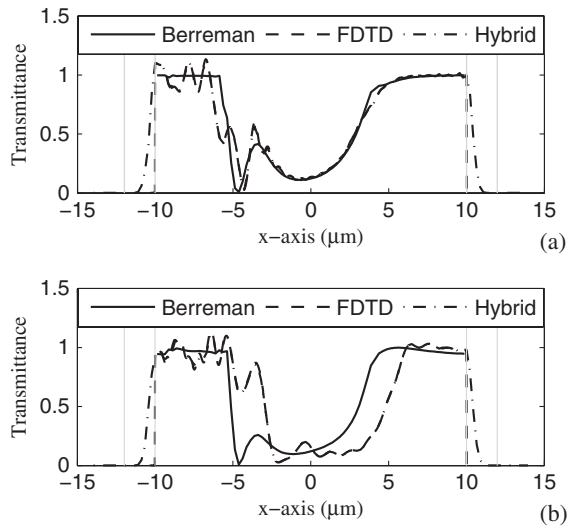

Figure 6. Transmittance along the x-axis in the on state ($V = 3V$) at (a) normal incidence and (b) 30° incidence. y-polarised incident light with $\lambda = 623.8$ nm, with y-transmitted analyser.

the light propagates through the twisted structures in the middle of Figure 4 because the guiding effect of polarisation for twist textures results in the transference of energy from the transverse electric mode to the transverse magnetic mode. When the light passes through either the left or right part of Figure 4, the energy transference is not evident, but the light propagates faster for the liquid crystal director tilted in the z direction in the presence of external electric fields. In addition, scattering and diffraction caused by the defect near the edge between the left half of the electrode and the space can be observed. The distribution of E_y at 30° incidence is also given in Figure 5(b).

To know more about the energy coupling and scattering/diffraction effect caused by the defect, an ideal analyser with the y-transmission optical axis in the near-field collection line was assumed instead of its implementation in the computational grid, and the transmittance in this collection line was evaluated. As shown in Figure 6, the transmittance calculated by the hybrid PSTD–FDTD and FDTD methods superpose each other in the total-field region. The maximum deviation of the transmittance obtained using both methods is less than 5.1%. In addition, the details of the energy fluctuations can be seen clearly for these methods taking the interactions between neighbour grids along the x direction into account, while the results obtained by the Berreman method failed to give this information.

Besides the accuracy of the hybrid PSTD–FDTD method, we are also interested in the improvement of the computational cost of the hybrid PSTD–FDTD method compared with that of the FDTD method. From theoretical analysis, the ratio of the memory requirement between the hybrid PSTD–FDTD and FDTD methods is $N^{\mathrm{h}}_{\lambda,x}/N^{\mathrm{f}}_{\lambda,x}$ for the same grid size Δz, where $N^{\mathrm{h}}_{\lambda,x}$ and $N^{\mathrm{f}}_{\lambda,x}$ refer to the grid sampling resolution ($\lambda/\Delta x$) of the hybrid PSTD–FDTD and FDTD methods in the x direction, respectively. Both the hybrid PSTD–FDTD and FDTD methods are adopted to simulate the propagation of light through the pixel for 100 fs on a Pentium(R) D 2.8 GHz processor/1 GB memory desktop computer. As shown in Table 1, the memory capacity and computational time required for the hybrid PSTD–FDTD method are about 8.5% and 21%, respectively, compared with those required for the FDTD method. This ratio of memory requirement varies slightly from the theoretical value, due to the fact that the number of the PML grid is fixed, and auxiliary variables require some memory capacity. With an increase of the liquid crystal cell aperture, the ratio of the memory requirement will approach the theoretical value. Meanwhile, the FFT calculation will further reduce the computational time of the hybrid PSTD–FDTD method.

Table 1. Comparison between time and memory required for hybrid and FDTD methods.

Method	Grid	$N_{\lambda,x}$	$N_{\lambda,z}$	Δt (fs)	Memory	Execution time
Hybrid	128×734	2.88	40	1.759×10^{-2}	31 MB	58 min
FDTD	1304×734	40	40	1.759×10^{-2}	365 MB	279 min

4. Conclusion

The hybrid PSTD–FDTD method is introduced to simulate the propagation of light through liquid crystals according to the characteristics of the thin plate structure of the liquid crystal cells. The FDTD method is applied to the thickness direction of a cell and the PSTD method is applied to the glass substrate direction, which will take advantage of the characteristics that the FDTD method is suitable for the modelling of an electrically small problem with fine structural details, while the PSTD method is suitable for the modelling of an electrically large problem with smooth internal media. The PMLs based on the ($\boldsymbol{D}$, $\boldsymbol{H}$) fields are used to truncate the open computational space including anisotropic media. The generalised TF/SF technique, combining the TF/SF technique of the FDTD method and the weighted TF/SF technique of the PSTD method, is used to introduce the plane-wave source. Numerical validation and comparison of the results from the hybrid PSTD–FDTD method, the FDTD method and the Berreman method are made for the same TN pixel in the on state for 100 fs. The maximum deviation of the transmittance obtained using both the hybrid PSTD–FDTD and FDTD methods is less than 5.1%; the memory capacity and computational time required for the hybrid PSTD–FDTD method are about 8.5% and 21%, respectively, compared with those required for the FDTD method. The results indicate that the hybrid PSTD–FDTD method is accurate, and also reduces the memory requirement and computational time of the FDTD method.

Acknowledgement

The authors thank the National Natural Science Foundation of China (No. 60878048) for its financial support.

References

[1] Jones, R.C. *J. Opt. Soc. Am.* **1941**, *31*, 488–493.
[2] Yeh, P. *J. Opt. Soc. Am.* **1982**, *72* (4), 507–513.
[3] Berreman, D.W. *J. Opt. Soc. Am.* **1972**, *62*, 502–510.
[4] Panasyuk, G.; Kelly, J.R.; Bos, P. *Liq. Cryst.* **2004**, *31*, 1503–1515.
[5] Olivero, D.; Oldano, C. *Liq. Cryst.* **2003**, *30*, 345–353.
[6] Kriezis, E.E.; Elston, S.J. *Appl. Opt.* **2000**, *39*, 5707–5714.
[7] Yee, K.S. *IEEE Trans. Antennas Propag.* **1966**, *14*, 302–307.
[8] Kriezis, E.E.; Elston, S.J. *Opt. Commun.* **1999**, *165*, 99–105.
[9] Titus, C.M. Refractive and Diffractive Liquid Crystal Beam Steering Devices. Ph.D. Dissertation, Kent State University, USA, 2000.
[10] Taflove, A.; Hagness, S.C. *Computational Electrodynamics: The Finite-Difference Time-Domain Method*, 3rd edn; Artech House Publishers: Boston, 2005.
[11] Liu, Q.H. *Microw. Opt. Technol. Lett.* **1997**, *15*, 158–165.
[12] Liu, Q.H. *IEEE Microw. Guided Wave Lett.* **1999**, *9*, 48–50.
[13] Leung, Y.F.; Chan, C.H. *Microw. Opt. Technol. Lett.* **1999**, *23*, 249–254.
[14] Li, Q.; Chen, Y.; Li, C.K. *Microw. Opt. Technol. Lett.* **2002**, *34*, 19–24.
[15] Gao, X.; Mirotznik, M.S.; Shi, S.Y.; Prather, D.W. 3D *Microw. Opt. Technol. Lett.* **2005**, *45*, 502–507.
[16] Zhao, A.P. *Microw. Opt. Technol. Lett.* **1998**, *17*, 164–168.
[17] Gao, X.; Mirotznik, M.S.; Prather, D.W. *IEEE Trans. Antennas Propag.* **2004**, *52*, 1665–1671.
[18] Garcia, S.G.; HungBao, T.M.; Martin, R.G.; Olmedo, B.G. *IEEE Trans. Microw. Theory Tech.* **1996**, *44*, 2195–2206.
[19] Moss, C.D.; Teixeira, F.L.; Kong, J.A. *IEEE Trans. Antennas Propag.* **2002**, *50*, 1174–1184.
[20] Oh, C.; Escuti, M.J. *Opt. Express* **2006**, *14*, 11870–11884.
[21] Fang, Y.; Wu, L.; Zhang, J. *IEEE Antennas Wirel. Propag. Lett.* **2009**, *8*, 414–417.
[22] Anderson, J.E.; Watson, P.E.; Bos, P.J. *LC3D: Liquid Crystal Display 3-D Director Simulation Software and Technology Guide*; Artech House Publishers: Boston, 2001.